Hindawi
Advances in Civil Engineering
Volume 2021, Article ID 8845329, 17 pages
https://doi.org/10.1155/2021/8845329

Research Article

Numerical Simulation of Basic Properties of Full-Steel Slag Aggregate Concrete

Zhu Bian,[1] Yuan Fang,[2] Feng Yu,[2] Xuliang Wang,[3] and Guosheng Xiang[2]

[1]*School of Architecture and Civil Engineering, West Anhui University, Lu'an 237012, Anhui, China*
[2]*Dept. of Civil Engineering and Architecture, Anhui University of Technology, Maanshan 243002, Anhui, China*
[3]*China MCC17 Group Co., Ltd., Ma'anshan 243000, Anhui, China*

Correspondence should be addressed to Feng Yu; fyuan86@163.com

Received 15 June 2020; Revised 18 November 2020; Accepted 7 December 2020; Published 21 January 2021

Academic Editor: Jorge Branco

In this study, the bit-level table of orthogonal test is adopted as the coding form of Genetic Algorithm (GA), and a Back Propagation (BP) neural network prediction model of the basic properties of full steel slag aggregate concrete (FSSAC) is established, and the experiment data are validated with good agreement. The impacts of several parameters including the sand ratio, water-cement ratio, content of steel slag sand, replacement particle size of steel slag sand, content of coarse steel slag, and replacement particle size of coarse steel slag on the compressive strength and expansion rate of the FSSAC are numerically investigated. The results show that the compressive strength of the FSSAC declines with the increase of the sand ratio, water-cement ratio, content of the steel slag sand, or coarse steel slag while it first increases and then decreases as the replacement particle size of steel slag sand or replacement particle size of coarse steel slag increases. The expansion rate of the FSSAC increases as the sand ratio or content of coarse steel slag increases. With a gradual increase of the water-cement ratio, content of steel slag sand, replacement particle size of steel slag sand, or replacement particle size of coarse steel slag, the expansion rate of the FSSAC first increases and then decreases. In addition, the impacts of the three most important parameters (i.e., water-cement ratio, content of steel slag sand, and replacement particle size of steel slag sand) on the stress-strain relationship of the FSSAC stub columns is further numerically studied.

1. Introduction

With the accelerating process of urbanization, the urban renovation and construction industry are rapidly flourishing, which make concrete one of the world's most widely used construction materials. The massive use of concrete consumes a large amount of natural aggregate, sand and gravel, etc., which is unfavorable to the environment and not conducive to the protection of the natural resources. Therefore, the search for a reasonable and effective substitute for concrete aggregate attracts the attention of scholars.

Steel slag is an industrial waste generated in the process of steel-making, which occupies about 15%~20% of the crude steel output. At present, the steel slag is mainly used as raw material for steel and iron, backfill material for road, admixture material for concrete, and so on [1–5]. The main chemical composition of the steel slag is similar to that of cement, as shown in Table 1 [6]. Using it to replace cement is a main direction of resource utilization of steel slag. Monshi Ahmad [7] used pulverized steel slag to produce steel slag Portland special cement and found that the prepared cement met the requirements of stability. Altun [8] added steel slag to ordinary Portland cement and demonstrated the strength and durability of the mixed cement conform to the Turkish TS standard. Li 9 carried out the tests on the durability of the steel slag cement and showed that the steel slag cement presented the advantages of high later strength, good durability, and slightly expanding. Mymrin [10] tested the hydration hardening products of the steel slag and showed that the gelling properties of the steel slag were good, which could be enhanced by adding a small amount of limestone. Wu [11] investigated the Portland cement with binary steel

Table 1: Chemical composition of the steel slag [6].

Chemical composition	C_aO (%)	SiO_2 (%)	Al_2O_3 (%)	Fe_2O_3 (%)	M_gO (%)	SO_3 (%)	TiO_2 (%)	M_nO (%)	P_2O_5 (%)
Steel slag	52.71	12.97	2.12	19.53	4.31	0.3	1.59	2.21	2.57

slag and fly ash and indicated that the strength could be up to 52.5 standard. The properties of the double mixing cement were small shrinkage, good durability, and slight swelling.

In view of certain hardness, fineness, and activity of steel slag, in recent years, some scholars have attempted to prepare steel slag aggregate concrete (SSAC) by using steel slag as concrete aggregate. Shi [12] investigated the basic performance of the SSAC and showed that the early compressive strength of the SSAC was low while the durability was good. Geng [13] studied the basic mechanical properties of the SSAC and revealed that the early activity of the SSAC was better than that of the fly ash and slag concrete. Anastasiou [14] recycled construction waste and electric furnace steel slag as coarse aggregate to produce low-strength concrete with part of the cement replaced by fly ash and demonstrated that with a small quantity of the steel slag, the low-strength concrete satisfied the requirements of the durability. Qasrawi et al. [15] conducted the experimental study to evaluate the suitability of the local unprocessed steel slag for use in normal concrete mixtures. The steel slag was adopted as fine aggregate substituting the sand in the mixtures, and five different replacement ratios (i.e., 0%, 15%, 30%, 50%, and 100%) were considered. The results demonstrated that the introduction of steel slag would increase the concrete strength, especially the tensile strength, provided the rational replacement ratio was adopted.

On the permeability and durability of the SSAC, Yang [16] tested the permeability of chloride ion through the SSAC and demonstrated that the permeability of chloride ion through the concrete with highly charged steel slag was similar to that of the ordinary concrete. Further, the permeability was significantly increased by adding an admixture, such as double mixing fly ash. For the concrete prepared with steel slag, researchers [17, 18] found that the durability properties such as water absorption, accelerated ageing, and porosity were smaller than those of the concrete prepared with natural aggregates. The results of Mo [19] showed that after CO_2 curing, the compressive strength of the SSAC increased remarkably.

On the expansion properties of the SSAC, Geiseler [20] found that when some f-CaO was in the concrete, the steel slag caused the concrete to expand in a short time. Chatterji [21] investigated the expansion mechanism of CaO and MgO in the steel slag and revealed that the expansion of steel slag was caused by the growth stress of the crystal and the diffusion effect from the dissolution of the oxide. When the contents of f-CaO and MgO in the steel slag were high, the hydration reaction of the steel slag caused the concrete to expand. Qian [22] found that for a steel slag that contained Fe, Mn, and MgO, MgO did not affect the stability of the steel slag, which could be estimated using the property parameter KM of the RO phase in the steel slag. Wang [23] derived a formula for the steel slag expansion force and applied a removable test device to measure the safety factor of the expansion stress.

It is well known that the steel slag contains MgO and f-CaO. Due to the expansion of MgO and f-CaO during hydration, the application of the SSAC in civil engineering is limited to some extent. The expansion property of the SSAC is obviously different from that of ordinary concrete. To further expand the application arrange of the SSAC, it is a feasible and reasonable selection to prepare the expansive-shrinkage self-balancing SSAC by properly using steel slag instead of the coarse aggregate or fine aggregate. This not only solves the contradiction between the supply and demand of natural aggregate, but also ensures the shrinkage compensating self-balancing properties of concrete. The expansive-shrinkage self-balancing SSAC shares the characteristics of small volume deformation, good stability, and excellent durability, which can significantly improve the working performance of concrete.

Orthogonal experimental design is one of the most widely used methods for studying and processing multifactor experiments, with the characteristic of "uniform dispersion, uniform comparability" [24]. Genetic algorithm is a parallel random search optimization method, which can imitate the natural genetic mechanism and evolutionary process. The individuals with high fitness value are retained by the genetic algorithm to form a new group that inherits the previous generation and is better than the previous generation, so as to iterate until certain requirements are met [25, 26]. Inspired by the biological nervous system, Back Propagation (BP) neural network is a method to calculate the gradient of nonlinear multi-layer network, which adopts the Widrow-Hoff learning algorithm and the nonlinear differentiable transfer function [27]. BP neural network consists of three layers as input layer, hidden layer and output layer. There are complete connections between the upper and lower layers, and no connections between the neurons in each layer.

In this study, the experimental data of the FSSAC are employed as the input sample of the Genetic Algorithm (GA), the bit-level table of orthogonal test is adopted as the coding form of the GA, the GA is used for optimization, a BP neural network model of the FSSAC is established, and the rationality of the prediction model is verified by the experimental data. On this basis, the impacts of the several parameters on the compressive strength, expansion rate, and stress-strain relationship of the FSSAC are numerically investigated.

2. BP Neural Network Prediction Model of Basic Properties of the FSSAC

2.1. Experiment Description. To reveal the influence of various studied parameters (i.e., sand ratio, water-cement ratio, content of steel slag sand, replacement particle size of steel slag sand, content of coarse steel slag, and replacement

particle size of coarse steel slag) on the basic properties of the FSSAC, the orthogonal tests of the compressive strength and expansion rate of the FSSAC are conducted. Twenty-five 100 mm × 100 mm × 300 mm tested blocks and twenty-five 100 mm × 100 mm × 100 mm cube tested blocks are designed and prepared. According to the method specified in the Chinese code GB/T 50081-2019 [28], 100 mm × 100 mm × 100 mm cube tested blocks are used to determine the compressive strength of the FSSAC and the continuous and uniform loading scheme are employed in the tests, and the loading speed is 0.5 MPa/s. With reference to the test method in the Chinese code GB/T50082-2009 [29], 100 mm × 100 mm × 300 mm tested blocks are adopted to measure the expansion rate of the FSSAC. The specific calculation formula of the expansion rate is as follows:

$$E_{xt} = \frac{(L_t - L_0)}{L_e}, \quad (1)$$

where E_{xt} means the t-th day expansion rate, L_e represents the gauge length of FSSAC, L_0 and L_t are the 3-day and t-th day length of FSSAC. The quantitative levels of each parameters, the bit-level table of orthogonal test, and experimental results are listed in Tables 2 and 3 [30, 31]. The amount of various materials of the FSSAC is listed in Table 4. Additionally, as depicted in Figure 1, eight 150 mm × 150 mm × 550 mm FSSAC stub columns are prepared and tested under axial compression, and the measured stress-strain relationship curves of the FSSAC stub columns are obtained.

2.2. BP Neural Network Prediction Model. To solve the problem that there is no clear mapping between the compressive strength and expansion rate of FSSAC and various studied parameters, a BP neural network is used as the main prediction model in this analysis. The nonlinear mapping relationship between the input layer and output layer is established by learning and training the bit-level table of orthogonal test and experimental results, as shown in Figure 2. The output value range of the BP neural network is [0, 1]. The test data are processed and the measured compressive strength and expansion rate of the FSSAC are, respectively, multiplied by the coefficients of 0.01 and 0.1 in this analysis. The structure of the BP neural network in this study is established based on Kosmogorov theorem, which is an empirical suggestion and can not be used to determine an accurate model. Therefore, the number of the hidden layer neurons of the model needs to be adjusted. In this study, 15, 20, 25, and 30 were taken as the number of hidden layer neurons, respectively, and 2, 7, 12, 17, and 22 groups were selected as trial data. The error curve is shown in Figure 3. It can be concluded that the error is minimum when the number of neurons in the hidden layer is 25.

2.3. BP Neural Network Model Optimized by Genetic Algorithm. BP neural network can not obtain the initial weights and biases quickly and accurately. To overcome this shortcoming, the GA is employed to optimize the neural network structure. The network structure parameters are taken as the optimization parameters, and the reciprocal of the squared sum of errors returned by the network model is taken as the fitness function for optimization. The detailed process is shown in Figure 4.

2.4. Verification of the BP Neural Network Prediction Model. To validate the rationality of the above-mentioned modified model, experimental data in this study and predicted results are compared in Table 5. Obviously, the experimental data of compressive strength and expansion rate of FSSAC agree well with the predicted results. Additionally, the comparisons between the model prediction results and the experimental data are shown in Table 6 and Figure 5. The comparisons between the measured and predicted values show that the model has acceptable precision, and most of the predicted ultimate stress and ultimate strain values are in good agreement with the experimental results.

2.5. Numerical Simulation of Compressive Strength of the FSSAC. In this section, the impacts of the sand ratio, water-cement ratio, content of steel slag sand, replacement particle size of steel slag sand, content of coarse steel slag, and replacement particle size of coarse steel slag on the compressive strength of the FSSAC are numerically investigated based on the above-mentioned prediction model. In the process of model analysis, due to the large dispersion of the compressive strength of the FSSAC, the GA is amplified to reduce the error of the prediction results, as shown in Figure 6. As can be seen from the figure, when the GA is greater than 60, the error variation tends to be stable.

2.6. Impact of Sand Ratio on the Compressive Strength. To reveal the impact of the sand ratio on the compressive strength of the FSSAC, the parameters are set as follows: the water-cement ratio is 0.58, contents of steel slag sand and coarse are 50% and 60%, replacement particle size of steel slag sand and coarse steel slag are the full particle size. The sand ratio is set as 34%, 36%, 38%, and 40%, respectively. As depicted in Figure 7, the compressive strength decreases with the increase of the sand ratio. This is mainly because in the case of unchanged dosage of cementing material, with the increase of sand ratio, the wrapping performance of cement mortar to coarse and fine aggregates is reduced, which weakens the adhesion between the coarse aggregate and fine aggregate, leading to the reduction of the compressive strength of the FSSASC [32, 33].

2.7. Impact of Water-Cement Ratio on the Compressive Strength. To analyze of the impact of water-cement ratio on the compressive strength of the FSSAC, the parameters are set as follows: the sand ratio is 0.38, contents of steel slag sand and coarse are 50% and 60%, and replacement particle size of steel slag sand and coarse steel slag are the full particle size. The water-cement ratio is set as 0.32, 0.38, 0.47, and 0.58, respectively. As illustrated in Figure 8, decreasing the water-cement ratio enhances the compressive strength of the

Table 2: The quantitative levels of each parameter [30, 31].

Level	Factor					
	Sand ratio A	Water-cement ratio B	Content of steel slag sand C (%)	Replacement particle size of steel slag sand D (mm)	Content of coarse steel slag E (%)	Replacement particle size of coarse steel slag F (mm)
1	34	0.58	0	Full particle size	0	Full particle size
2	36	0.58	25	0.15~0.3	0	2.36~4.75
3	38	0.47	50	0.3~0.6	30	4.75~9.5
4	38	0.38	75	0.6~1.18	60	9.5~16.0
5	40	0.32	100	1.18~2.36	100	>16.0

Table 3: The bit-level table of the orthogonal test and test results.

ID	Sand ratio A	Water-cement ratio B	Content of steel slag sand (%) C	Replacement particle size of steel slag sand (mm) D	Content of coarse steel slag (%) E	Replacement particle size of coarse steel slag (mm) F	Compressive strength (28d) (MPa)	Expansion rate (30d) (10^{-4})
1	1	1	1	1	1	1	34.5	−2.26
2	1	2	2	2	2	2	36.5	1.95
3	1	3	3	3	3	3	34.1	3.62
4	1	4	4	4	4	4	34.5	1.10
5	1	5	5	5	5	5	44.3	0.63
6	2	1	2	3	4	5	26.9	1.56
7	2	2	3	4	5	1	23.5	−0.65
8	2	3	4	5	1	2	44.5	−4.20
9	2	4	5	1	2	3	40.8	1.16
10	2	5	1	2	3	4	60.6	4.21
11	3	1	3	5	2	4	33.7	1.36
12	3	2	4	1	3	5	25.5	1.51
13	3	3	5	2	4	1	20.3	1.08
14	3	4	1	3	5	2	32.1	1.59
15	3	5	2	4	1	3	47.4	2.45
16	4	1	4	2	5	3	11.9	−0.20
17	4	2	5	3	1	4	17.5	1.07
18	4	3	1	4	2	5	41.3	−1.7
19	4	4	2	5	3	1	45.5	−0.40
20	4	5	3	1	4	2	34.8	0.02
21	5	1	5	4	3	2	21.5	1.84
22	5	2	1	5	4	3	29.2	−1.87
23	5	3	2	1	5	4	31.7	−0.676
24	5	4	3	2	1	5	26.1	2.88
25	5	5	4	3	2	1	40.3	0.65

FSSAC. This may come from that with the decrease of water-cement ratio, the free water between solid particles decreases, resulting in the reduction of pores formed in the concrete hardening process, and the corresponding decrease of porosity, thereby enhancing the compressive strength of the FSSAC [34].

2.8. Impact of the Content of Steel Slag Sand on the Compressive Strength. To examine the impact of the content of steel slag sand on the compressive strength of the FSSAC, the parameters are set as follows: the sand ratio is 0.38, water-cement ratio is 0.58, content of coarse steel slag is 60%, and replacement particle size of steel slag sand and coarse steel slag are the full particle size. The content of steel slag sand is set as 0, 25%, 50%, 75%, and 100%, respectively. As shown in Figure 9, obviously, the compressive strength decreases as the content of steel sand increases. This is mainly because the fineness modulus of the steel slag sand is smaller than that of the ordinary sand, and the increase in the content of steel slag sand enhances the void rate and the specific surface area while decreasing the package area of cement.

2.9. Impact of Replacement Particle Size of Steel Slag Sand on the Compressive Strength. To analyze of the impact of the replacement particle size of steel slag sand on the compressive strength of the FSSAC, the parameters are set as follows: the sand ratio and water-cement ratio are 0.38, 0.58, contents of steel slag sand and coarse steel slag are 50% and 60% and replacement particle size of coarse steel slag is the full particle size. The replacement particle size of steel slag

Table 4: Amount of various materials of the FSSAC (kg/m^3).

Specimen ID	Ordinary sand (kg)	Steel slag sand (kg)	Coarse steel slag (kg)	Coarse aggregate (kg)	Cement (kg)	Water (kg)
1	616	0	1195	0	345	200
2	462	154	1195	0	345	200
3	296	296	803	344	426	200
4	140	420	435	653	526	200
5	0	531	0	1030	625	200
6	489	163	463	695	345	200
7	326	326	0	1158	345	200
8	157	470	1113	0	426	200
9	0	593	1054	0	526	200
10	562	0	699	300	625	200
11	344	344	1122	0	345	200
12	172	516	785	337	345	200
13	0	660	431	646	426	200
14	626	0	0	1022	526	200
15	445	148	967	0	625	200
16	172	516	0	1122	345	200
17	0	688	1122	0	345	200
18	660	0	1077	0	426	200
19	469	157	715	307	526	200
20	297	297	387	580	625	200
21	0	724	760	326	345	200
22	724	0	434	651	345	200
23	521	175	0	1042	426	200
24	330	330	988	0	526	200
25	156	467	935	0	625	200

Figure 1: The FSSAC stub columns and cube test blocks.

sand is set as full particle size, 0.15 mm~0.3 mm, 0.3 mm~0.6 mm, 0.6 mm~1.18 mm, and 1.18 mm~2.36 mm, respectively. As can be seen from Figure 10, when the replacement particle size of steel slag sand is larger than 0.3, the compressive strength increases as the replacement particle size of steel slag sand increases. This is mainly because the skeleton function of concrete aggregate and interfacial bond strength enhance with the increase of the replacement particle size of steel slag sand. When the replacement particle size of steel slag sand is smaller than 0.3, the compressive strength slightly decreases with the increase of the replacement particle size of steel slag sand.

2.10. Impact of the Content of Coarse Steel Slag on the Compressive Strength. To reveal the impact of the content of coarse steel slag on the compressive strength of the FSSAC, the parameters are set as follows: the sand ratio and water-cement ratio are 0.38 and 0.58, content of steel slag sand is 50%, replacement particle size of steel slag sand and coarse steel slag are the full particle size. The content of coarse steel slag is 0, 30%, 60% and 100%, respectively. Figure 11 depicts the impact of the content of coarse steel slag on the compressive strength of the FSSAC. Apparently, the compressive strength of FSSAC declines as the content of coarse steel slag increases. This is mainly because the void rate increases as

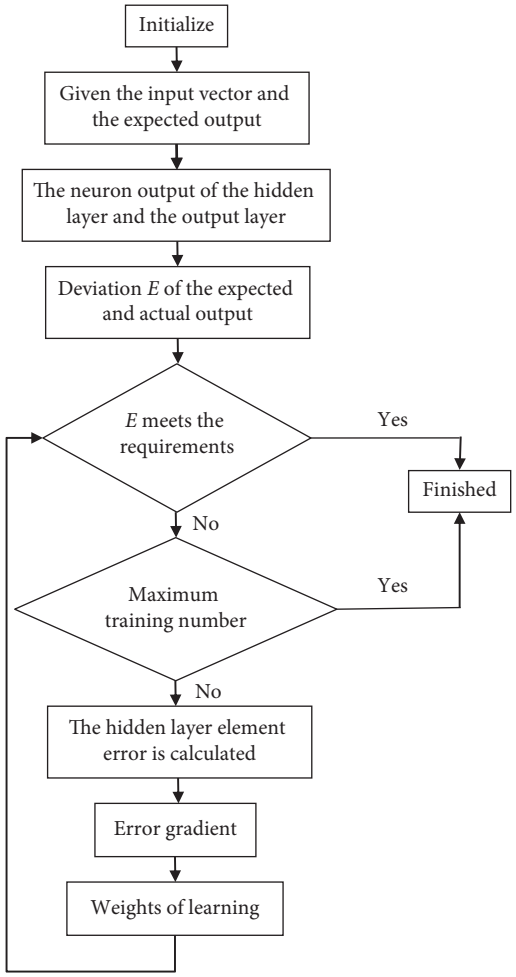

Figure 2: BP neural network flow chart.

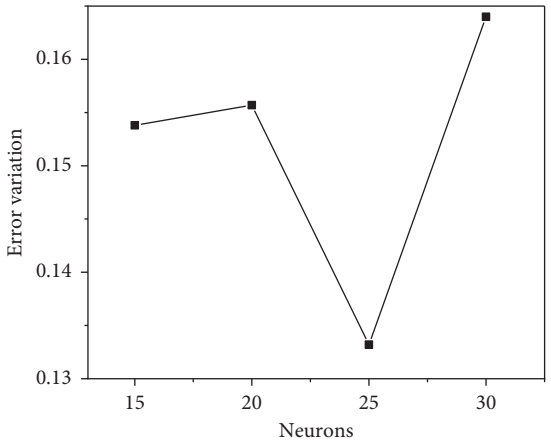

Figure 3: Error curve.

the content of coarse steel slag increases and the crushing value of the steel slag is lower than the ordinary gravel.

2.11. Impact of the Replacement Particle Size of Coarse Steel Slag on the Compressive Strength. To examine the impact of the replacement particle size of coarse steel slag on the compressive strength of the FSSAC, the parameters are set as follows: the sand ratio and water-cement ratio are 0.38 and 0.58, contents of steel slag sand and coarse steel slag are 50% and 60%, and replacement particle size of steel slag sand is full particle size. The replacement particle size of coarse steel

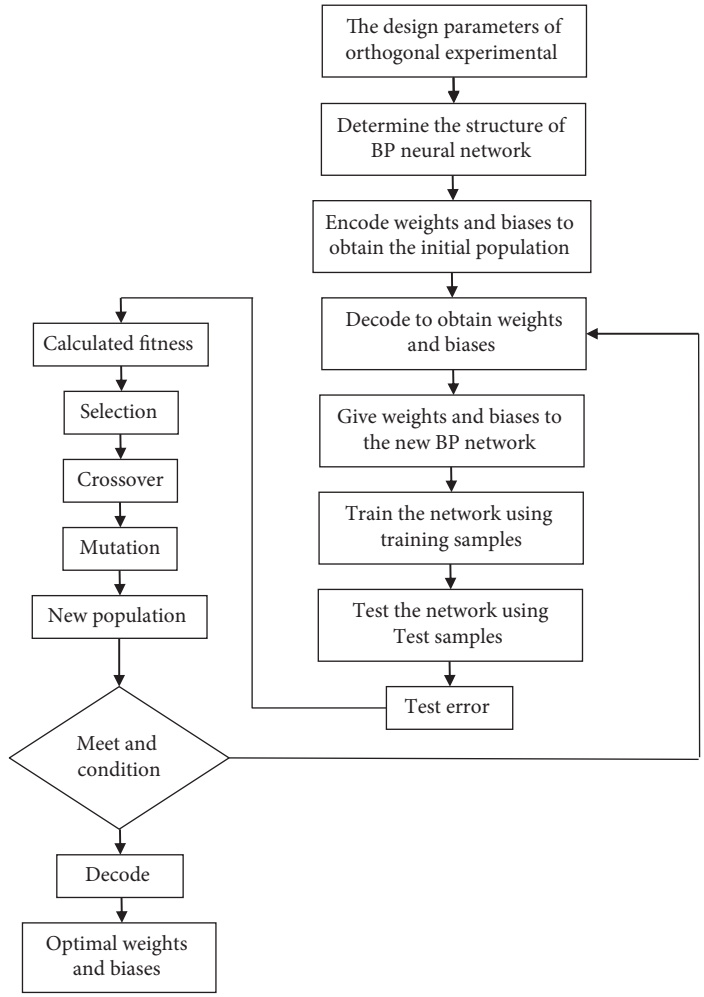

Figure 4: Flow chart of the BP neural network optimized by genetic algorithm.

Table 5: Comparison between the experimental data of the compressive strength and expansion rate of the FSSAC with the predicted results.

Mechanical property	Compressive strength (MPa)			Expansion rate (10^{-4})		
ID	Measured	Predicted	Error (%)	Measured	Predicted	Error (%)
2	36.5	37.4	2.5	1.95	1.94	0.5
4	34.5	32.9	4.6	1.10	1.12	1.8
5	44.3	42.1	5.0	0.63	0.64	1.6
13	20.3	21.0	3.4	1.08	1.06	1.9
21	21.5	22.5	4.7	1.84	1.87	1.6

Table 6: Comparisons between the model prediction results and the experimental data.

Specimen		Ultimate stress (10^4 N/mm^2)			Ultimate strain (10^{-3})					
					Transverse			Axial		
Water-cement ratio	ID	Measured	Calculated	Error (%)	Measured	Calculated	Error (%)	Measured	Calculated	Error (%)
0.58	ZS1	27.13	27.51	1.4	1.76	1.73	1.7	0.57	0.53	7.2
	ZS2	28.45	25.72	9.6	1.54	1.61	4.5	0.64	0.60	6.3
0.47	ZS3	15.98	17.35	8.6	1.60	1.67	4.4	0.39	0.36	7.7
	ZS4	28.49	29.72	4.3	1.69	1.53	9.5	0.55	0.52	5.5
0.38	ZS5	35.85	28.47	20.6	1.94	1.65	14.9	0.36	0.41	13.9
	ZS6	31.24	30.58	2.1	1.21	1.31	8.3	0.43	0.45	4.7
0.32	ZS7	36.83	30.59	16.9	1.72	1.39	19.2	0.53	0.52	1.9
	ZS88	35.58	29.18	18.0	1.77	1.51	14.7	0.72	0.62	13.9

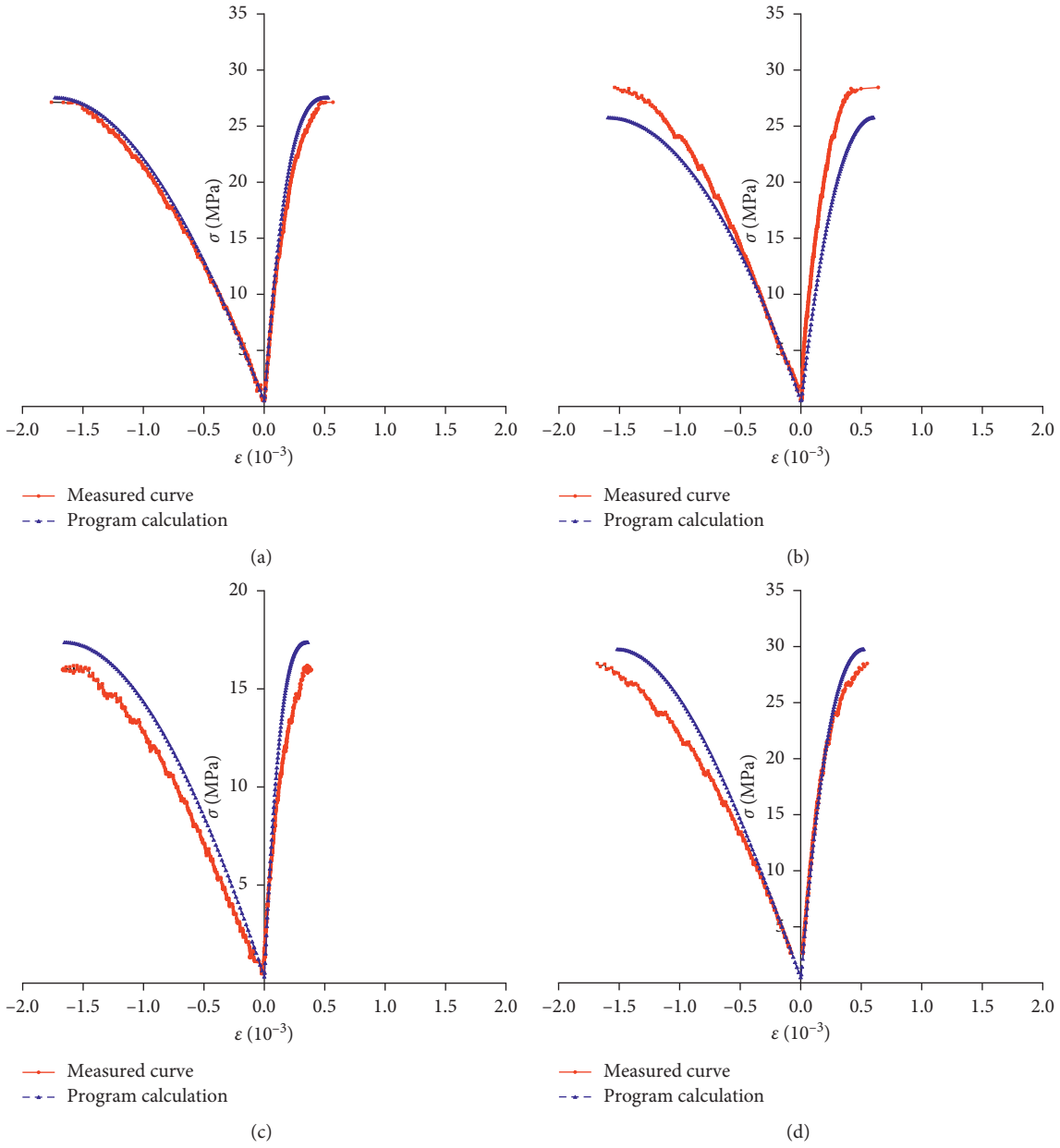

Figure 5: Continued.

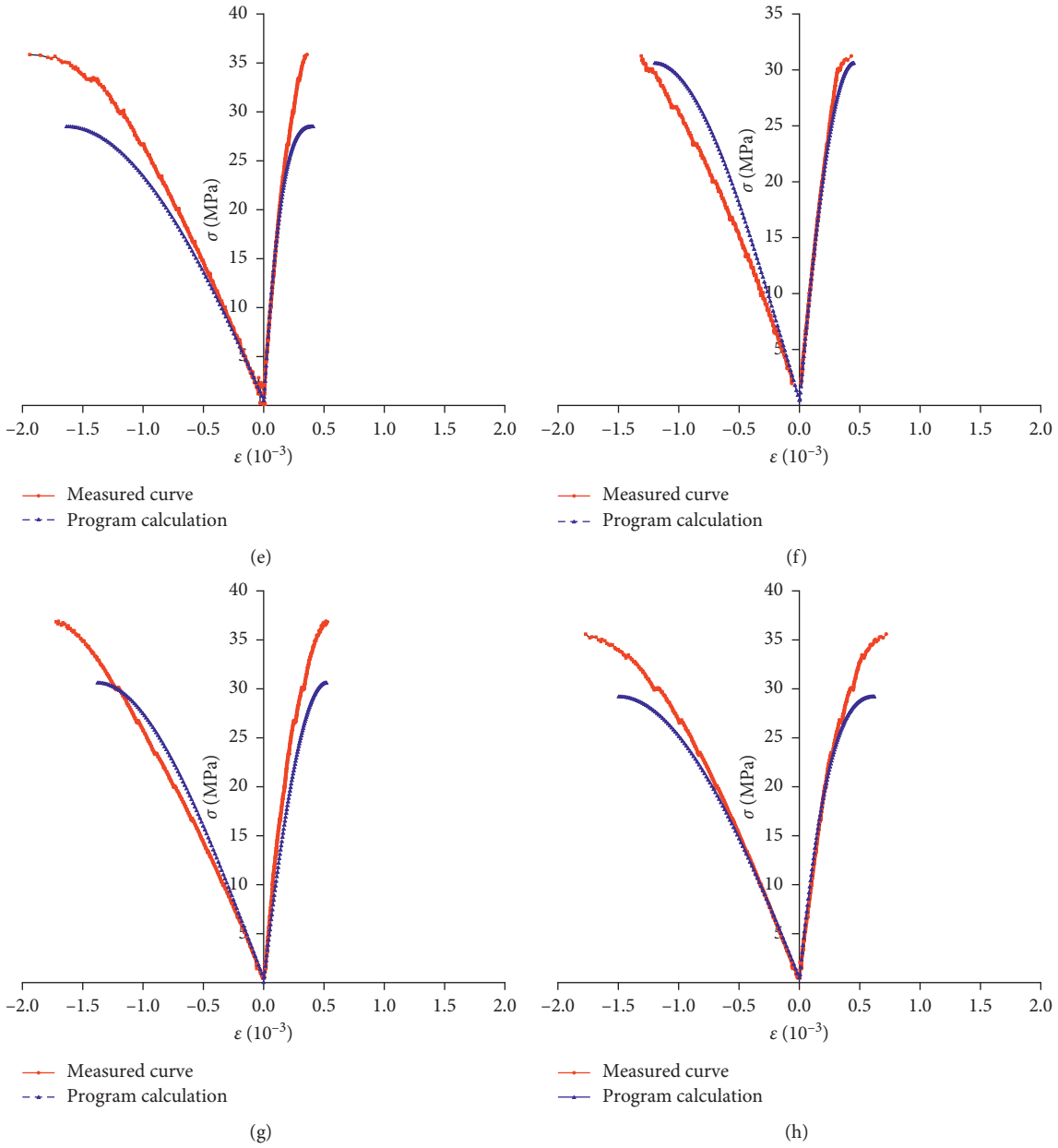

Figure 5: Comparisons between the model predicted stress-strain curves and measured curves. (a) ZS1. (b) ZS2. (c) ZS3. (d) ZS4. (e) ZS5. (f) ZS6. (g) ZS7. (h) ZS8.

slag is set as full particle size, 0.15 mm~0.3 mm, 0.3 mm~0.6 mm, 0.6 mm~1.18 mm, and 1.18 mm~2.36 mm, respectively. As illustrated in Figure 12, the compressive strength of the FSSAC first decreases and then increases as the replacement particle size of coarse steel slag increases. The reason is that when the replacement particle size of coarse steel slag is marginal, the aggregate strength of steel slag slightly decreases with the increase of the replacement particle size of coarse steel slag. The aggregate strength of steel slag and concrete interface connection strength increase as the replacement particle size of coarse steel slag increases.

2.12. Numerical Simulation of the Expansion Rate of the FSSAC. In this section, the impacts of the sand ratio, water-cement ratio, content of steel slag sand and coarse steel slag, replacement particle size of steel slag sand, and coarse steel slag on the expansion rate of the FSSAC are numerically investigated based on the developed analysis model. The GA and error variation is shown in Figure 13.

2.13. Impact of Sand Ratio on the Expansion Rate. To reveal the impact of the sand ratio on the expansion rate of the FSSAC, the parameters are set as follows: the water-cement ratio is 0.58, contents of steel slag sand and coarse steel slag are 50% and 60%, replacement particle size of steel slag sand and coarse steel slag are the full particle size. The sand ratio is set as 34%, 36%, 38%, and 40%, respectively. Figure 14 depicts the impact of the sand ratio on the expansion rate

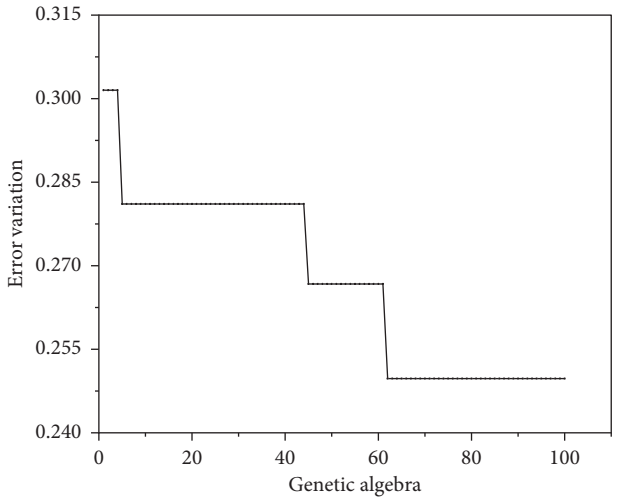

Figure 6: The genetic algebra and error variation of the compressive strength of the FSSAC.

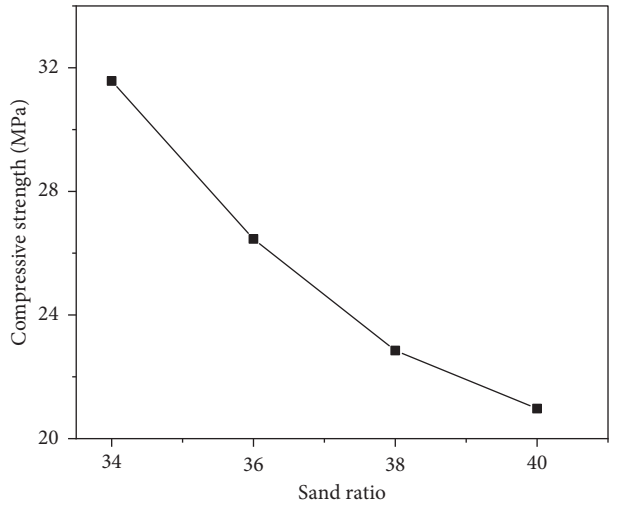

Figure 7: The impact of the sand ratio on the compressive strength of the FSSAC.

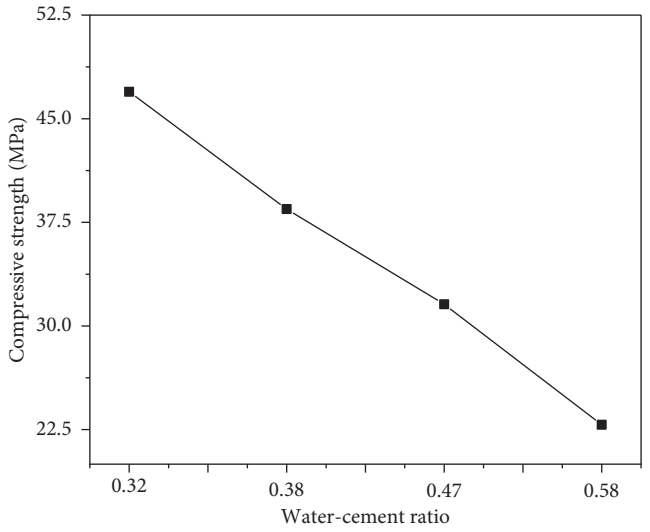

Figure 8: The impact of the water-cement ratio on the compressive strength of the FSSAC.

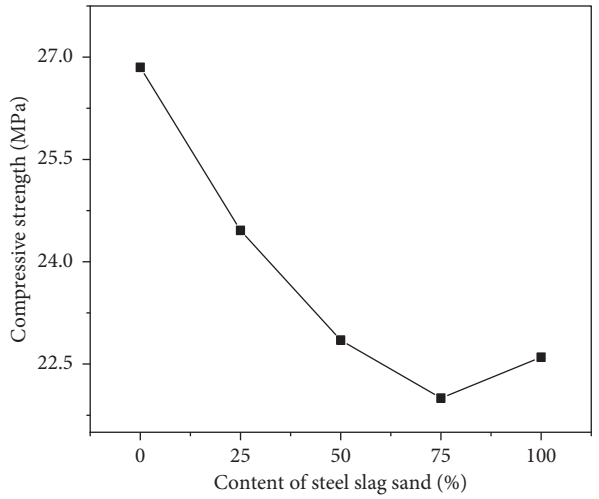

Figure 9: The impact of the content of steel slag sand on the compressive strength of the FSSAC.

of the FSSAC. Clearly, the expansion rate of the FSSAC gradually increases with the increase of the sand ratio. The reason is that increasing the sand ratio, the content of the steel slag sand increases gradually and correspondingly enhances the expansion effect of the steel slag.

2.14. Impact of Water-Cement Ratio on the Expansion Rate. To analyze of the impact of the water-cement ratio on the expansion rate of the FSSAC, the parameters are set as follows: the sand ratio is 0.38, contents of steel slag sand and coarse steel slag are 50% and 60%, and replacement particle size of steel slag sand and coarse steel slag are the full particle size. The water-cement ratio is set as 0.32, 0.38, 0.47, and 0.58, respectively. As shown in Figure 15, the expansion rate of the FSSAC increases first and then decreases with the increase of the water-cement ratio. This may come from that the expansion stress enhances as the water-cement ratio increases in certain range. As the water-cement ratio further increases, the shrinkage deformation of the FSSAC increases obviously and correspondingly decreases the expansion deformation.

2.15. Impact of the Content of Steel Slag Sand on the Expansion Rate. To examine the impact of the content of steel slag sand on the expansion rate of the FSSAC, the parameters are set as follows: the sand ratio and water-cement ratio are 0.38 and 0.58, content of coarse steel slag is 60%, and replacement particle size of steel slag sand and coarse steel slag are the full particle size. The content of steel slag sand is set as 0, 25%, 50%, 75%, and 100%, respectively. As depicted in Figure 16, the expansion rate of the FSSAC first increases and then decreases with the increase of the content of steel slag sand. The reason is that the expansion stress produced by steel slag

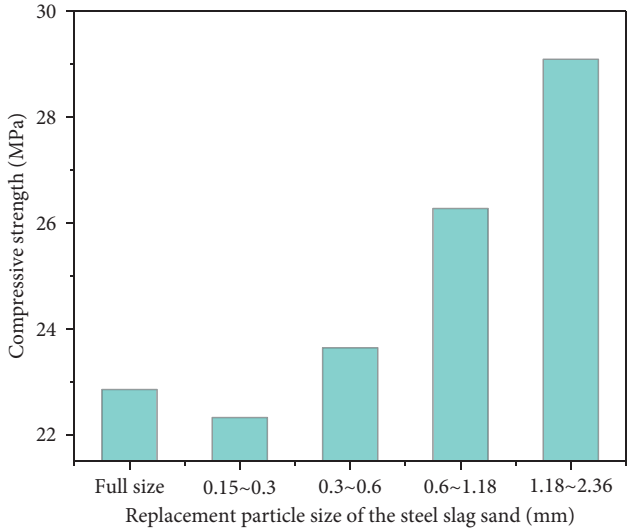

Figure 10: The impact of the replacement particle size of steel slag sand on the compressive strength of the FSSAC.

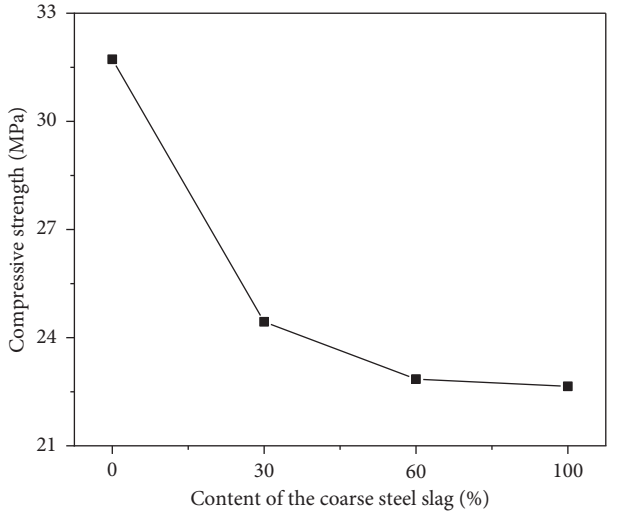

Figure 11: The impact of the content of coarse steel slag on the compressive strength of the FSSAC.

sand increases with the increase of the content of steel slag sand. With the further increases in the content of steel slag sand, the redundant steel slag sand can not take part in the alkali aggregate reaction.

2.16. Impact of Replacement Particle Size of Steel Slag Sand on the Expansion Rate. To analyze of the impact of the replacement particle size of steel slag sand on the expansion rate of the FSSAC, the parameters are set as follows: the sand ratio and water-cement ratio are 0.38, 0.58, contents of steel slag sand and coarse steel slag are 50% and 60%, and replacement particle size of coarse steel slag is the full particle size. The replacement particle size of steel slag sand is set as full particle size, 0.15 mm~0.3 mm, 0.3 mm~0.6 mm, 0.6 mm~1.18 mm, and 1.18 mm~2.36 mm, respectively. As can be seen from Figure 17, the expansion rate of the FSSAC

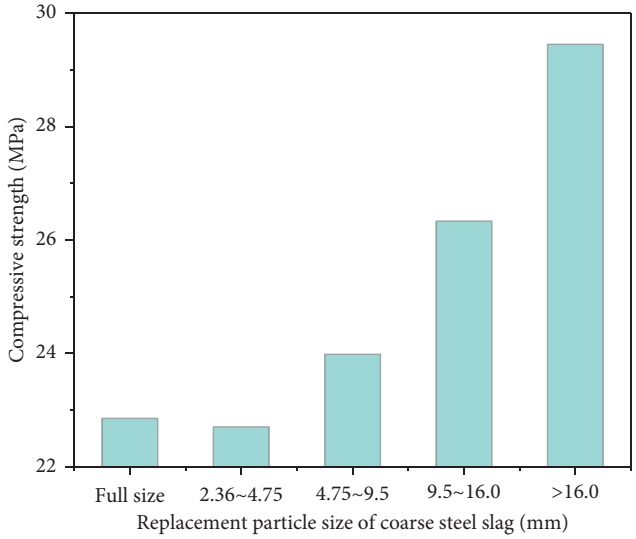

Figure 12: The impact of the replacement particle size of coarse steel slag on the compressive strength of the FSSAC.

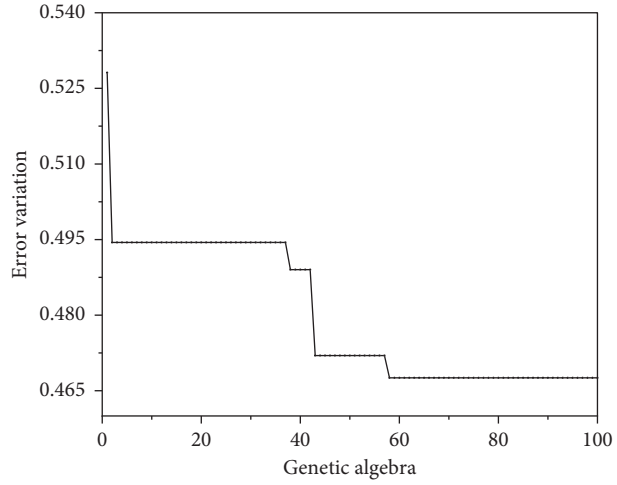

Figure 13: The genetic algebra and error variation of the expansion rate of the FSSAC.

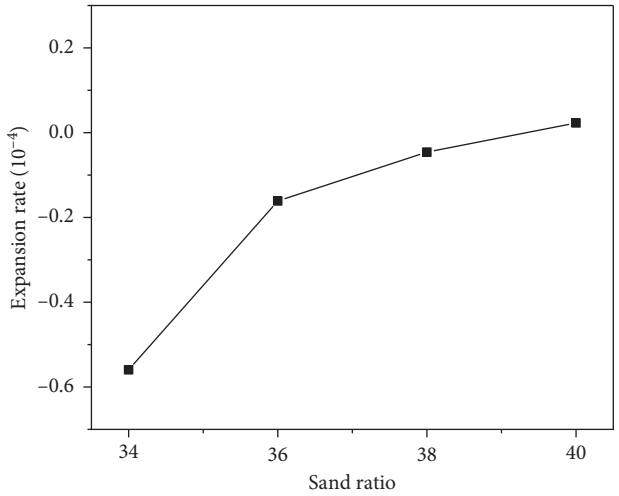

Figure 14: The impact of the sand ratio on the expansion rate of the FSSAC.

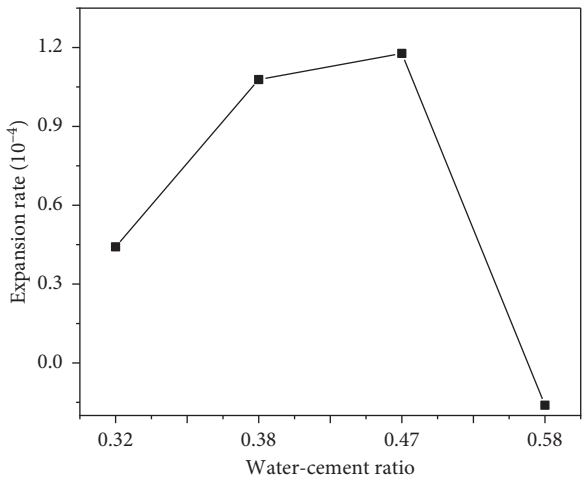

Figure 15: The impact of the water-cement ratio on the expansion rate of the FSSAC.

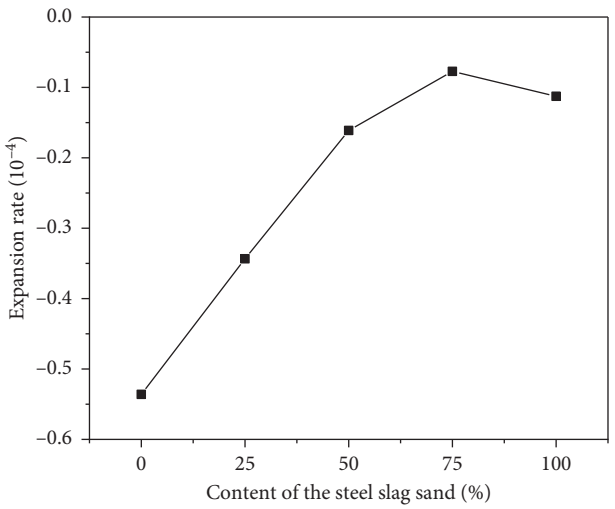

Figure 16: The impact of the content of steel slag sand on the expansion rate of the FSSAC.

increases first and then decreases with the increase of the replacement particle size of steel slag sand. This indicates that when the replacement particle size of steel slag sand is less than 0.6 mm, the activity of steel slag can be fully developed, and the steel slag can completely participate in the alkali aggregate reaction of concrete. When the replacement particle size of steel slag is larger than 0.6 mm, the specific surface area of steel slag gradually decreases, and the activity of steel slag is not fully developed and the expansion rate of the FSSAC decreases accordingly.

2.17. Impact of Content of Coarse Steel Slag on the Expansion Rate. To reveal the impact of the content of coarse steel slag on the expansion rate of the FSSAC, the parameters are set as follows: the sand ratio and water-cement ratio are 0.38 and 0.58, content of steel slag sand is 50%, and replacement particle size of steel slag sand and coarse steel slag are full particle size. The content of coarse steel slag is 0, 30%, 60%, and 100%, respectively. As illustrated in Figure 18, apparently, the expansion rate of the FSSAC increases as the content of coarse steel slag increases. This is mainly because, in contrast, the steel slag has a relatively large porosity, and the crushing value is lower than the ordinary gravel.

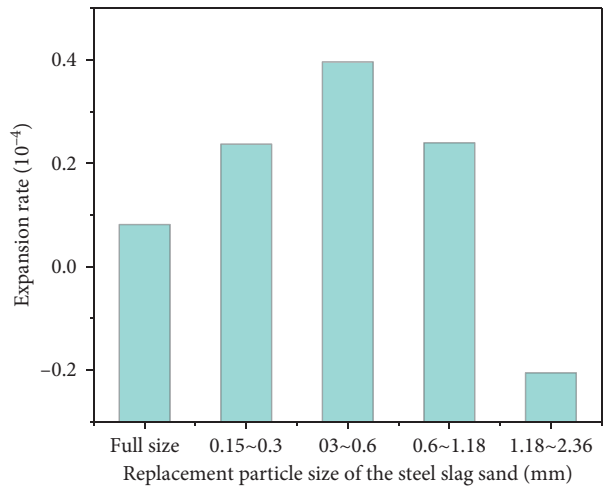

Figure 17: The impact of the replacement particle size of steel slag sand on the expansion rate of the FSSAC.

2.18. Impact of Replacement Particle Size of Coarse Steel Slag on the Expansion Rate. To examine the impact of the replacement particle size of coarse steel slag on the expansion rate of the FSSAC, the parameters are set as follows: the sand ratio and water-cement ratio are 0.38 and 0.58, contents of steel slag sand and coarse steel slag are 50% and 60%, and replacement particle size of steel slag sand is full particle size. The replacement particle size of coarse steel slag is set as full particle size, 0.15 mm~0.3 mm, 0.3 mm~0.6 mm, 0.6 mm~1.18 mm, and 1.18 mm~2.36 mm, respectively. As shown in Figure 19, the expansion rate of the FSSAC first increases and then decreases as the replacement particle size of coarse steel slag increases. This is mainly because when the replacement particle size is marginal, the appropriate increase of the replacement particle size of the coarse steel slag is beneficial to the alkali aggregate reaction of the FSSAC. With the further increase of the replacement particle size of coarse steel slag, the specific surface area reduces, correspondingly decreasing the expansion rate of the FSSAC.

3. Numerical Simulation of the Stress-Strain Relationship of the FSSAC Stub Columns

According to the test results, among the six studied parameters, the water-cement ratio, content of steel slag sand, and replacement particle size of steel slag sand have more obvious impacts on the mechanical properties of the FSSAC. In this section, the impacts of these three parameters on the stress-strain relationship of the FSSAC stub columns are further analyzed based on the verified numerical model.

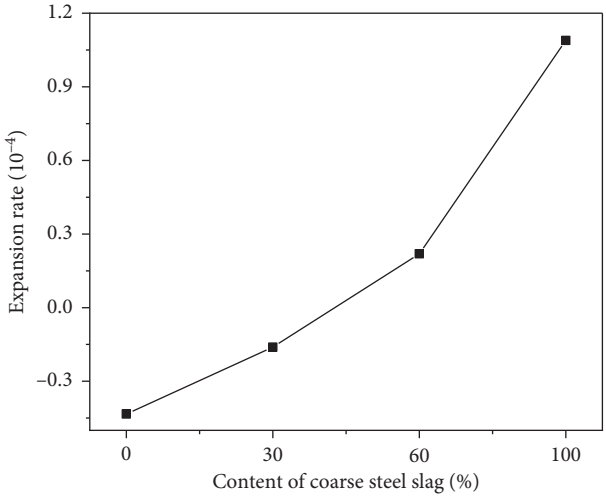

Figure 18: The impact of the content of coarse steel slag sand on the expansion rate of the FSSAC.

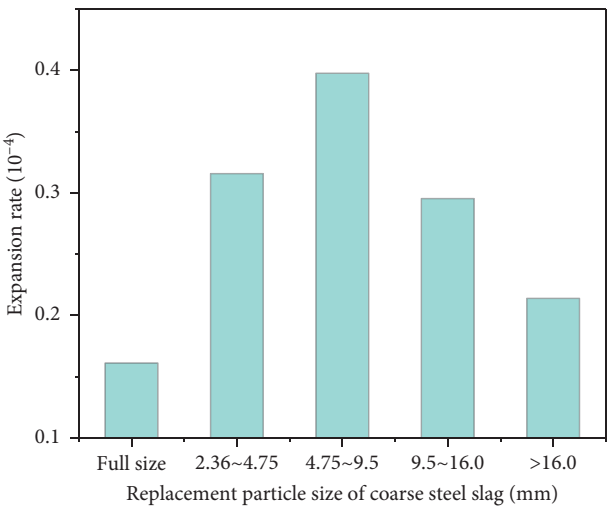

Figure 19: The impact of the replacement particle size of coarse steel slag on the expansion rate of the FSSAC.

3.1. Impact of Water-Cement Ratio. In order to analyze the impact of the water-cement on the stress-strain relationship of the FSSAC stub columns, the parameters are set as follows: the sand ratio is 38%, content of steel slag sand is 50%, replacement particle size of steel slag sand is the average particle size corresponding to the fineness modulus, content of coarse steel slag is 50%, and replacement particle size of coarse steel slag is the average particle size of the continuous gradation. The water-cement ratio is set as 0.3, 0.35, 0.4, 0.45, 0.5, 0.55, and 0.60, respectively. The impact of the water-cement ratio on the ultimate stress of the FSSAC stub columns is demonstrated in Figure 20. It can be seen that the ultimate stress of the FSSAC stub columns decreases with the increase of the water-cement ratio. The rates of decrease at lower and higher water-cement ratios are faster than that at the medium water-cement ratio.

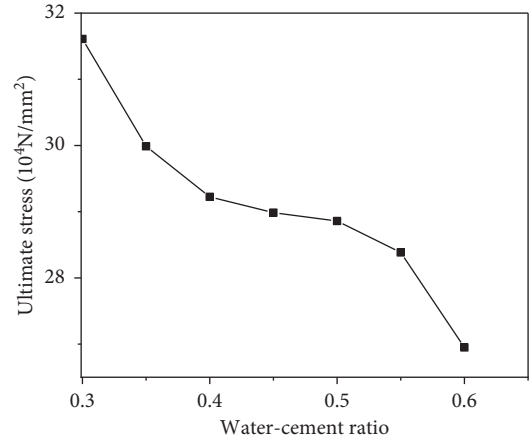

Figure 20: The impact of the water-cement ratio on the ultimate stress of the FSSAC stub columns.

Figure 21 illustrates the impact of the water-cement ratio on the ultimate strains of the FSSAC stub columns. It can be seen from Figure 21(a) that when the water-cement ratio is relatively small or large, the impact of the water-cement ratio on the ultimate axial strain of the FSSAC stub columns is obvious, and the ultimate axial strain of the FSSAC stub columns increases significantly with the increase of the water-cement ratio. In contrast, the impact of the water-cement ratio on the ultimate transverse strain of the FSSAC stub columns is not obvious, as shown in Figure 21(b).

Figure 22 shows the impact of the water-cement ratio on the stress-strain relationship curves of the FSSAC stub columns. It can be seen that during the initial stage of loading, all the stub columns are in the elastic phases and the stress-strain curves are approximately linear. The elastic stages of the specimens are longer due to the few internal defects and small holes in the specimens. At this stage, the slope of the axial stress-strain curves decreases with the increase of the water-cement ratio, but there are no distinct differences among the stress-strain curves. Then, as the load increases, the elastic modulus of the FSSAC decreases and the stress-strain curves of the specimens are no longer straight line. The slope of the axial stress-strain curves decreases significantly with the increase of the water-cement ratio. In contrast, the water-cement ratio has little impact on the transverse stress-strain curves. When the stress in the specimens reaches the ultimate stress, the axial strain and transverse strain increase rapidly. At this moment, the increase in the water-cement ratio causes a decrease in the ultimate stress and elastic modulus, and an increase in the ultimate axial strain, but only a minor variation in the transverse strain. The slope of the stress-strain curves is gentle.

3.2. Impact of the Content and Replacement Particle Size of the Steel Slag Sand. In order to analyze the impact of the content and replacement particle size of steel slag sand on the stress-strain relationship of the FSSAC stub columns, the parametersare set as follows: the sand ratio is 38%, water-cement ratio is 0.47, content of coarse steel slag is

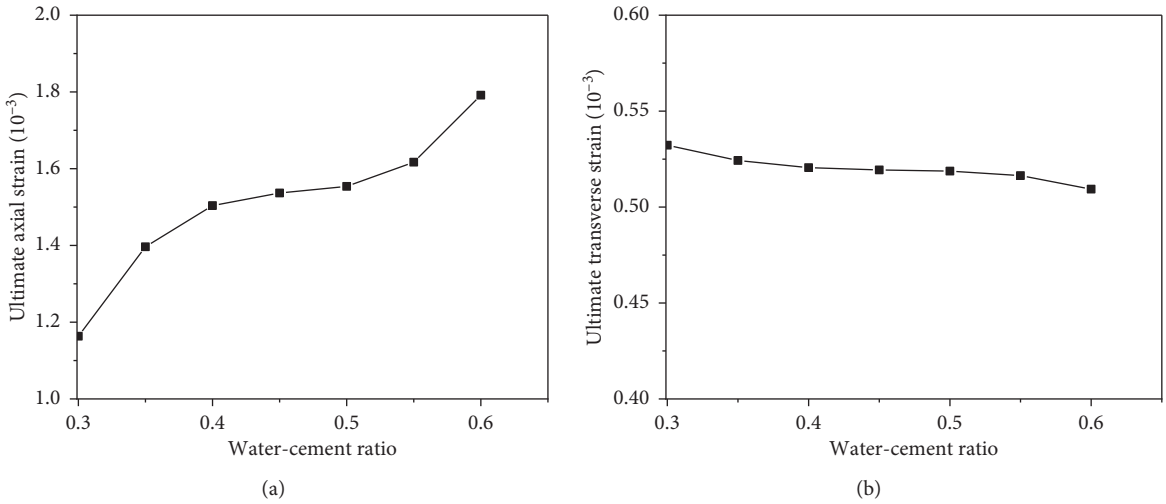

Figure 21: The impact of the water-cement ratio on the ultimate strains of the FSSAC stub columns. (a) Ultimate axial strain. (b) Ultimate transverse strain.

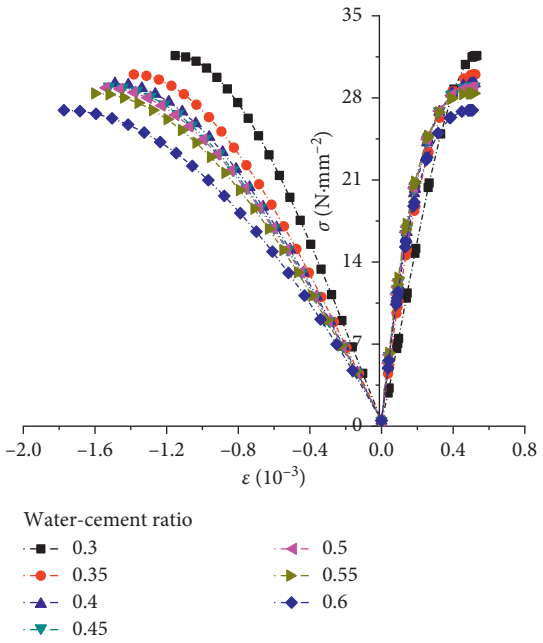

Figure 22: The impact of the water-cement ratio on the stress-strain curves of the FSSAC stub columns.

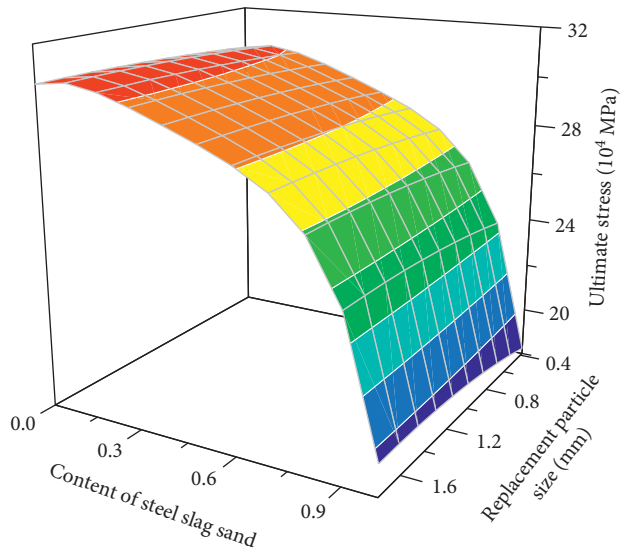

Figure 23: The impact of the content and replacement particle size of steel slag sand on the ultimate stress.

50%, and replacement particle size of coarse steel slag is the average particle size of the continuous gradation.

Figure 23 shows the impact of the content and replacement particle size of steel slag sand on the ultimate stress of the FSSAC stub columns. Apparently, an increase in the content of steel slag sand causes a decrease in the ultimate stress of the FSSAC stub columns, and vice versa. On the other hand, the ultimate stress of the FSSAC stub columns increases with the increase of the replacement particle size of steel slag sand.

Figure 24 describes the impact of the content and replacement particle size of steel slag sand on the ultimate strains of the FSSAC stub columns. As can be seen from Figure 24(a), the ultimate axial strain of the FSSAC stub columns increases faster and faster with increasing the content of steel slag sand. Further, the ultimate axial strain increases with no obvious tendency with the increase of the replacement particle size of steel slag sand. As shown in Figure 24(b), it can be seen that the increase in the content of the steel slag sand causes a decrease in the ultimate transverse strain of the FSSAC stub columns and the rate of decrease increases gradually. The impact of the replacement particle size of the steel slag sand on the ultimate transverse strain of the FSSAC stub columns is not obvious.

Figure 25 shows the impact of the content of steel slag sand on the stress-strain relationship of the FSSAC stub columns. It can be seen that during the early loading period,

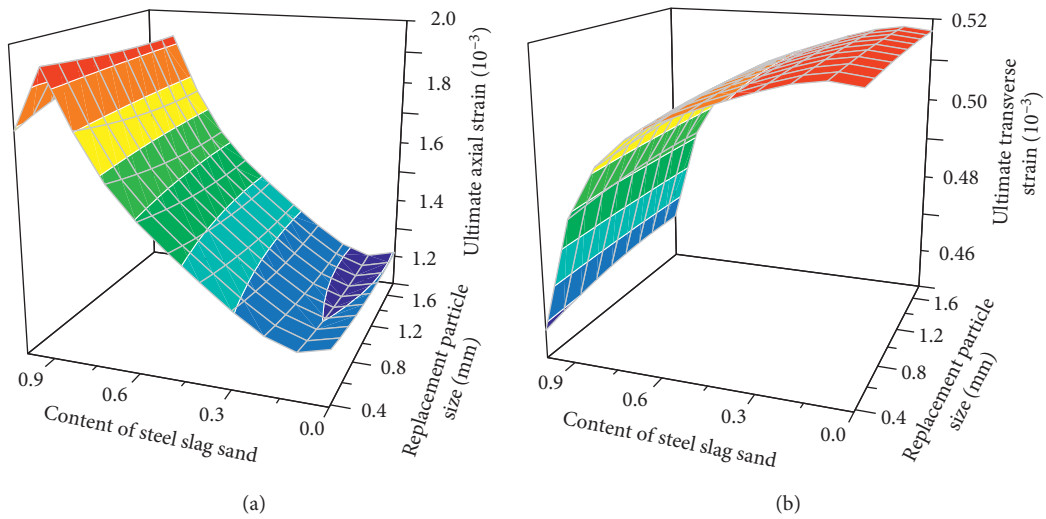

FIGURE 24: The impact of the content and replacement particle size of steel slag sand on the ultimate strains. (a) Ultimate axial strain. (b) Ultimate transverse strain.

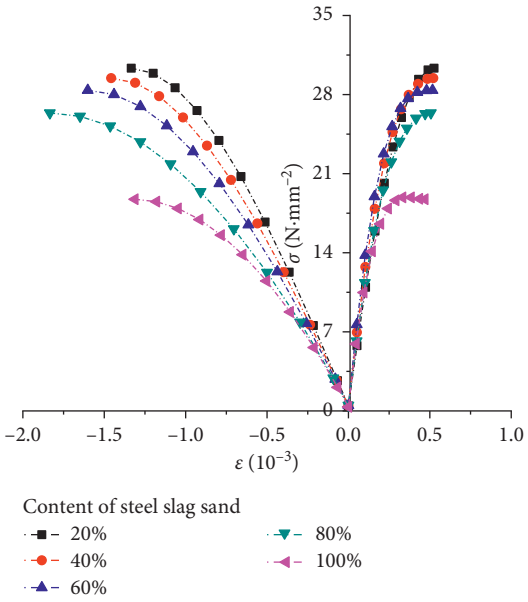

FIGURE 25: The impact of the content of steel slag sand on the stress-strain curves.

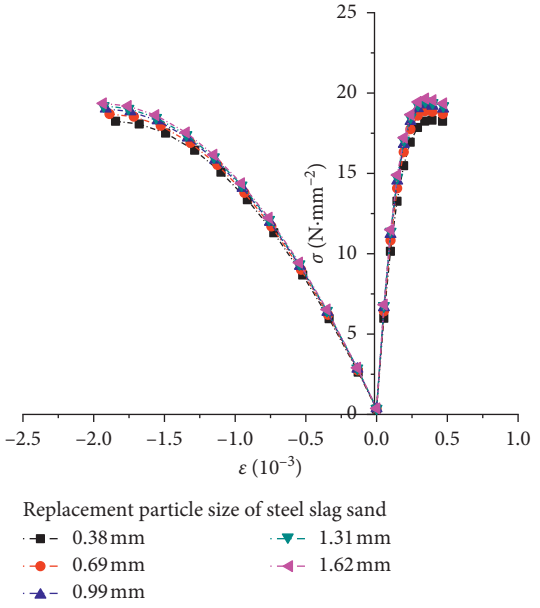

FIGURE 26: The impact of the replacement particle size of steel slag sand on the stress-strain curves.

the stub columns are in the elastic phase, the stress-strain curves are approximately straight lines. An increase in the content of steel slag sand may cause a decline in the slope of the axial stress-strain curves, even though there are no distinct differences among the stress-strain relationship curves. Then, with the further increase in loading, the specimens enter the elastic-plastic phase. The slope of the axial stress-strain curves decreases rapidly as the content of steel slag sand increases, and there are obvious differences among the axial stress-strain curves. On the other hand, the differences in the transverse stress-strain curves are quite small. When the stress in the specimens reaches the ultimate stress, the specimens are destroyed, and the axial strain and transverse strain increase rapidly. Further, the ultimate stress and elastic modulus of the FSSAC stub columns decrease, and the ultimate axial strain enhances with the increase of the content of steel slag sand. The differences among the transverse strains are still small, and the stress-strain curves are gentle.

Figure 26 shows the impact of the replacement particle size of steel slag sand on the stress-strain relationship of the FSSAC stub columns. It can be seen that the axial and transverse strains may decline with the increase of the replacement particle size of the steel slag sand. However, the

differences among the axial or transverse stress-strain relationship curves are fairly small.

4. Conclusions

In this study, a BP neural network prediction model of the basic properties of the FSSAC is established, and the experiment data are validated with good agreement. The impacts of the several parameters on the compressive strength, expansion rate, and stress-strain relationship of the FSSAC are numerically investigated based on the developed prediction model. Based on the numerical analysis results, the following conclusions can be drawn:

(1) The compressive strength of the FSSAC decreases with the increase of the sand ratio, content of steel slag sand, or coarse steel slag. Decreasing the water-cement ratio will enhance the compressive strength of the FSSAC. The compressive strength of the FSSAC first decreases and then increases with the increase of the replacement particle size of steel slag sand or coarse steel slag.

(2) The expansion rate of the FSSAC increases with the increase of the sand ratio or content of coarse steel slag. The expansion rate of the FSSAC first increases and then decreases with the increase of the water-cement ratio, content of steel slag sand, replacement particle size of steel slag sand, or coarse steel slag.

(3) The ultimate stress of the FSSAC stub columns decreases with increasing the water-cement ratio while the ultimate axial strain increases significantly with the increase of the water-cement ratio. However, the impact of the water-cement ratio on the ultimate transverse strain of the FSSAC stub columns is not obvious. The increase in the water-cement ratio will reduce the slope of the axial stress-strain curves while the water-cement ratio has little impact on the transverse stress-strain curves.

(4) The ultimate stress of the FSSAC stub columns decreases as the content of steel slag sand increases while the ultimate axial strain increases faster and faster with the increase of the content of steel slag sand. The increase in the content of steel slag sand causes a decrease in the ultimate transverse strain of the FSSAC stub columns and the rate of decrease increases gradually. The slope of the axial stress-strain curves of the FSSAC stub columns decreases rapidly with the increase of the content of steel slag sand, while the impact of content of steel slag sand on the transverse stress-strain curves is not distinct.

(5) The ultimate stress of the FSSAC stub columns increases with the increase of the replacement particle size of steel slag sand. The ultimate axial strain increases with no obvious tendency with the increase of the replacement particle size of steel slag sand. The impact of the replacement particle size of steel slag sand on the ultimate transverse strain of the FSSAC stub columns is not obvious. The replacement particle size of the steel slag sand has little impact on the axial and transverse stress-strain curves of the FSSAC stub columns.

Data Availability

The data used to support the findings of this study are included within the article.

Conflicts of Interest

The authors declare no conflicts of interest.

Acknowledgments

This study was sponsored by the National Natural Science Foundation of China (Nos. 51578001, 51878002, and 52078001), Outstanding Youth Fund of Anhui Province (No. 2008085J29), Key Research and Development Plan of Anhui Province (No. 1704a0802131), the University Synergy Innovation Program of Anhui Province (No.GXXT-2019-005), Key Project of West Anhui University (WXZR201814), Anhui Provincial Scientific Research Projects in Universities of Department of Education (KJ2018A412 and KJ2020A0234), and University-Level Quality Engineering Project of West Anhui University (wxxy2019075, wxxy2019023, and wxxy2019038).

References

[1] B. Das, S. Prakash, P. S. R. Reddy, and V. N. Misra, "An overview of utilization of slag and sludge from steel industries," *Resources, Conservation and Recycling*, vol. 50, no. 1, pp. 40–57, 2007.

[2] R. I. Iacobescu, D. Koumpouri, Y. Pontikes, R. Saban, and G. N. Angelopoulos, "Valorisation of electric arc furnace steel slag as raw material for low energy belite cements," *Journal of Hazardous Materials*, vol. 196, pp. 287–294, 2011.

[3] P. E. Tsakiridis, G. D. Papadimitriou, S. Tsivilis, and C. Koroneos, "Utilization of steel slag for Portland cement clinker production," *Journal of Hazardous Materials*, vol. 152, no. 2, pp. 805–811, 2008.

[4] H. Yi, G. Xu, H. Cheng, J. Wang, Y. Wan, and H. Chen, "An overview of utilization of steel slag," *Procedia Environmental Sciences*, vol. 16, pp. 791–801, 2012.

[5] V. Ducman and A. Mladenovič, "The potential use of steel slag in refractory concrete," *Materials Characterization*, vol. 62, no. 7, pp. 716–723, 2011.

[6] Y. Feng, F. Yuan, Z. Yang, X. Lin, and B. Rui, "Mechanical behavior of self-stressing steel slag aggregate concrete filled steel tubular stub columns," *Structural Concrete*, vol. 21, no. 1, pp. 1597–1611, 2020.

[7] M. S. Ahmad, "Producing portland cement from iron and steel slags and limestone," *Cement and Concrete Composites*, vol. 4, pp. 28-29, 1999.

[8] I. A. Altun and I. Yilmaz, "Study on steel furnace slags with high MgO as additive in Portland cement," *Cement and Concrete Research*, vol. 12, pp. 1247–1249, 2002.

[9] D. X. Li and X. H. Fu, "Durability study of steel slag cement," *Cement and Concrete Composites*.vol. 27, pp. 983–987, 1997.

[10] V. A. Mymrin, H. A. Ponte, and C. I. Yamamoto, "Synthesis of new colloidal formations during the strengthening of different

activated hydrated metallurgical slags," *Colloids and Surfaces A: Physicochemical and Engineering Aspects*, vol. 220, no. 1–3, pp. 211–221, 2003.

[11] X. Q. Wu, H. Zhu, X. K. Hou, and H. S. Li, "Study on steel slag and fly ash composite Portland cement," *Cement and Concrete Composites.*vol. 7, pp. 1103–1106, 1999.

[12] C. Shi and J. Qian, "High performance cementing materials from industrial slags-a review," *Resources, Conservation and Recycling*, vol. 29, no. 3, pp. 195–207, 2000.

[13] H. N. Geng and Q. Li, "Development of microstructure and chemical composition of hydration products of slag activated by ordinary Portland cement," *Materials Characteriaztion*, vol. 87, pp. 49–58, 2014.

[14] E. Anastasiou, K. Georgiadis Filikas, and M. Stefanidou, "Utilization of fine recycled aggregates in concrete with fly ash and steel slag," *Construction and Building Materials*, vol. 50, pp. 154–161, 2014.

[15] H. Qasrawi, F. Shalabi, and I. Asi, "Use of low CaO unprocessed steel slag in concrete as fine aggregate," *Construction and Building Materials*, vol. 23, no. 2, pp. 1118–1125, 2009.

[16] Y. B. Yang, S. Liang, H. H. Mo, and Y. W. Chen, "Chloride penetration resistance of concrete with multiplex-slag after 3 years of exposure in seawater environment," *China Civil Engineering of Journal*, vol. 4, pp. 92–94, 2006.

[17] J. M. Manso, J. J. Gonzalez, and J. A. Polanco, "Electric arc furnace slag in concrete," *Journal of Materials in Civil Engineering*, vol. 16, no. 6, pp. 639–645, 2004.

[18] P. Carlo, C. Paolo, F. Flora, and B. Katya, "Properties of concretes with black oxidizing electric arc furnace slag aggregate," *Cement and Concrete Composites*, vol. 37, pp. 232–240, 2013.

[19] L. Mo, F. Zhang, M. Deng, F. Jin, A. Al-Tabbaa, and A. Wang, "Accelerated carbonation and performance of concrete made with steel slag as binding materials and aggregates," *Cement and Concrete Composites*, vol. 83, pp. 138–145, 2017.

[20] H. M. J. Geiseler, "Products of steel slags an opportunity to save natural resources," *Waste Management*, vol. 3, pp. 285–293, 2001.

[21] S. Chatterji, "Mechanism of expansion of concrete due to presence of dead-burnt CaO and MgO," *Cement and Concrete Research*, vol. 25, pp. 51–56, 2006.

[22] G. R. Qian, D. D. Sun, J. H. Tay, and Z. Y. Lai, "Hydrothermal reaction and autoclave stability of Mg bearing RO phase in steel slag," *British Ceramic Transactions*, vol. 101, no. 4, pp. 159–164, 2002.

[23] G. Wang, "Determination of the expansion force of coarse steel slag aggregate," *Construction and Building Materials*, vol. 24, no. 10, pp. 1961–1966, 2010.

[24] R. J. Liu, Y. W. Zhang, C. W. Wen, and J. Tang, "Study on the design and analysis methods of orthogonal experiment," *Experimental Technology and Management*, vol. 9, pp. 52–55, 2010.

[25] Z. R. Yuan, *Artificial Neural Network and its Application*, Tsinghua university press, Beijing, China, 1999.

[26] Y. Liu, *Non-Numerical Parallel Algorithm-Genetic Algorithm*, Tsinghua university press, Beijing, China, 1995.

[27] H. Y. Wu, B. G. Chang, and C. C. Zhu, "A special case of genetic algorithm-orthogonal experimental design method," *Journal of Software*, vol. 1, pp. 148–153, 2006.

[28] GB/T 50081-2019, *Standard for Test Methods of Concrete Physical and Mechanical Properties*, National Standards of People's Republic of China, Beijing, China, 2019.

[29] GB/T50082-2009, *Standard for Test Methods of Long-Term Performance and Durability of Ordinary Concrete*, Ministry of Urban-Rural Development, Republic of China, Beijing, China, 2009.

[30] F. Yu, Y. Zhang, X. L. Wang et al., "Experimental study on compressive strength of full steel slag aggregate concrete," *Journal of Basic Science and Engineering*, vol. 26, no. 4, pp. 854–862, 2018.

[31] F. Yu, X. L. Wang, Y. Zhang et al., "Stress-strain relationship of shrinkage compensating steel-slag concrete," *Journal of Building Materials*, vol. 20, no. 4, pp. 527–534, 2017.

[32] W. T. Lin, "Effects of sand/aggregate ratio on strength, durability, and micro-structure of self-compacting concrete," *Construction and Building Materials*, vol. 242, pp. 1–14, 2020.

[33] M. L. Zhou and G. J. Ke, "Influence of sand ratio on the workability and compressive strength of concrete with coal gangue power," *Concrete*, vol. 8, pp. 133–135, 2016.

[34] E. Rahmani, M. K. Sharbatdar, and H. A. Beygi, "A comprehensive investigation into the effect of water to cement ratios and cement contents on the physical and mechanical properties of Roller Compacted Concrete Pavement (RCCP)," *Construction and Building Materials*, vol. 253, pp. 1–20, 2020.